



# Biaxial mechanical behavior of closed-cell aluminum foam under combined shear–compression loading

Zhi-bin LI<sup>1</sup>, Xue-yan LI<sup>1</sup>, Yu-xuan ZHENG<sup>2</sup>

1. College of Liberal Arts and Sciences, National University of Defense Technology, Changsha 410073, China;

2. State Key Laboratory of Explosion Science and Technology,

Beijing Institute of Technology, Beijing 100081, China

Received 16 April 2019; accepted 26 November 2019

**Abstract:** Combined shear–compression tests and simulations were performed on a closed-cell aluminum foam over a wide range of loading angles in order to probe their yield behaviors under biaxial loading conditions. Combined shear–compression tests were carried out by using a pair of cylindrical bars with beveled ends. The yield surfaces were experimentally measured and compared with various theoretical yield surface models. The cellular structures of closed-cell aluminum foams were modeled as tetrakaidecahedrons and their biaxial crushing behaviors were simulated by the finite element method. The results show that, yield initiates from the stress-concentrated corners in the specimens under combined shear–compression loading and the stress distribution is no longer uniform at the specimen/bar interfaces. In the range of cell sizes studied, the larger the foam cell size is, the higher the yield stress is. Aluminum foam density is found to be the dominant factor on its mechanical properties compared with the cell size and is much more significant in engineering practice.

**Key words:** combined shear–compression; closed-cell aluminum foam; yield surface; biaxial loading; yield behavior

## 1 Introduction

Metallic foams have been widely employed in aerospace and automotive industries due to their ultra-light weight, excellent energy absorption capability and other attractive mechanical characteristics [1,2], and thus have attracted great interest. Most often, aluminum foams are used in primary load bearing members and are subjected to multi-axial stress states, especially combined shear–compression. Therefore, there are growing demands to model accurately the mechanical behaviors and exploit the full potential of these ultra-light energy-absorbing materials in complex loading conditions.

Recently, a number of previous studies have been focused on the characteristics of mechanical properties and energy absorption of aluminum foams under various conditions, such as uniaxial [3,4], multi-axial [5,6] and indentation tests [7,8], as functions of loading rate and temperature. Mechanical properties of aluminum foams in simple stress states have been studied extensively, while their mechanical properties in complex stress states have been much less documented.

RUAN et al [9] conducted triaxial compressive experiments on CYMAT closed-cell aluminum foams with a test system consisting of an MTS, an ELE-Hoek cell and a modified ENERPAC pump. ZHOU et al [10,11] employed the Arcan test rig

**Foundation item:** Project (2017JJ3359) supported by the Natural Science Foundation of Hunan Province, China; Project (KFJJ13-11M) supported by the Opening Project of State Key Laboratory of Explosion Science and Technology (Beijing Institute of Technology), China

**Corresponding author:** Zhi-bin LI; Tel: +86-731-84573276; Fax: +86-731-84573297; E-mail: [lizhibin@nudt.edu.cn](mailto:lizhibin@nudt.edu.cn)

DOI: 10.1016/S1003-6326(19)65178-2

consisting of two pairs of plane semi-circular loading plates to obtain the initial yield behavior of closed-cell aluminum foams under combined shear–compression loading. KOSSA [12] proposed a biaxial compression test fixture made of two comb-like steel parts which can slide into each other. MOSLEH et al [13] developed a combined shear–compression testing comprising of two independent displacement actuators which apply the compression and shear displacements simultaneously in two orthogonal axes. The applications of these apparatuses have accumulated important experimental results for multiaxial loading of foams. However, these experimental devices are somewhat too complicated. Recently, a relatively simple and convenient combined shear–compression loading technique has been developed by adding cushions with designed oblique surfaces and has been successfully applied for PBXs [14], PMMA [15] and rock material [16].

Additional numerical simulations can provide more information about the foam material characteristics, in which the first task required is that the cell structure of the foam in three dimensions is well defined. A tetrakaidecahedron model was developed, of which the complete cell was composed of six squares and eight hexagons [17]. The tetrakaidecahedron model can reflect the geometric characteristics of foam materials and can fill the whole space perfectly, thus is an ideal model for studying the mechanical properties of low-density foam materials. MILLS and ZHU [18] studied the high strain compression properties of a closed-cell polymer foam using the tetrakaidecahedron model. GRENESTEDT [19] analyzed the tetrakaidecahedron structure together with a number of other models and concluded that, the tetrakaidecahedron model is a good model for closed-cell PVC foams.

Plastic collapse of the cell walls is the dominating yield mechanism for aluminum foams. Moreover, the initial yield of aluminum foams may be determined by probing a yield surface, which is a convex envelope in the stress space and the foam material remains elastic within the envelope while plastic deformation takes place on the envelope [9]. GIBSON et al [20], MILLER [21], and DESHPANDE and FLECK [22] proposed different yield criteria for metallic foams as

$$\Phi = \pm \frac{\sigma_e}{\sigma_{pl}} + 0.81 \left( \frac{\rho_f}{\rho_s} \right) \left( \frac{\sigma_m}{\sigma_{pl}} \right)^2 - 1 \leq 0 \quad (1)$$

$$\Phi = \sigma_e - \gamma p + \frac{\alpha'}{d_0 \sigma_c} p^2 - d_0 \sigma_c \leq 0 \quad (2)$$

$$\Phi = \frac{1}{1 + (\alpha/3)^2} [\sigma_e^2 + \alpha^2 \sigma_m^2] - \sigma_Y^2 \leq 0 \quad (3)$$

where  $\Phi$  is the yield function;  $\sigma_e$  is the von Mises effective stress;  $\sigma_{pl}$  is the magnitude of the uniaxial compression plateau strength;  $\rho_f$  is the initial density of the foam;  $\rho_s$  is the initial density of the fully dense solid material;  $\sigma_m$  is the mean stress;  $\gamma$  is a phenomenological yield surface parameter, of which the value is dictated by the ratio of uniaxial yield strengths;  $p$  is the pressure;  $\alpha'$  is also a phenomenological yield surface parameter;  $d$  corresponds to the uniaxial strength of the material;  $\alpha$  is the aspect ratio of the ellipse;  $\sigma_Y$  is the uniaxial strength.

Even though the yield surfaces of metallic foams have been extensively studied both experimentally and numerically, some ambiguous problems still exist. In the present study, the shear–compression mechanical properties of closed-cell aluminum foams are studied through performing experiments and numerical simulations. Firstly, by adding beveled bars and a column sleeve, quasi-static shear–compression experiments are conducted on a closed-cell aluminum foam. Then, LS-DYNA is employed to implement numerical simulations of the shear–compression process of closed-cell aluminum foams. Finally, the influences of two important parameters of aluminum foams, i.e. density and cell size, on the yield surface are discussed.

## 2 Experimental

### 2.1 Materials and specimens

A commercially available closed-cell aluminum foam (supplied by Osenter Metal Composite Materials Co., Ltd., Shanghai, China) with the average cell size of approximately 2 mm is used in the present study, which is produced by liquid state processing using titanium hydride (TiH<sub>2</sub>, 1–3 wt.%) as a foaming agent [23]. The cylindrical foam specimens with dimensions of  $d32 \text{ mm} \times 10 \text{ mm}$  are cut from a block, of which the cellular structure is examined to be almost homogeneous and the

average cell size is nearly constant. Density of the foam specimen changes from 0.45 to 0.55 g/cm<sup>3</sup> for nearly 100 samples, and the specimen density distribution is similar to normal distribution. Thus, the specimens which have a density of 0.49 g/cm<sup>3</sup> with a variability (defined as the standard deviation normalized by the mean value) of 8% are used in the experiments.

Details of the aluminum foam specimens are shown in Table 1. Size effects of closed-cell aluminum foams have already been demonstrated earlier experimentally [24]. Precautions have also been taken to eliminate the size effects in the present study. The size effect can be avoided if the foam plate has at least five cell diameters in thickness according to ANDREWS et al [25]. In the present study, the dimension of foam specimens is at least five times larger than the cell size in each direction. In this case, no significant effect of cell size on compression response will be noticed.

**Table 1** Specimen size and loading conditions of aluminum foam specimens

Diameter/ mm	Height/ mm	Density/ (g·cm <sup>-3</sup> )	Loading angle/ (°)	Loading speed/ (mm·min <sup>-1</sup> )
32.50	9.88	0.490	10	1
31.92	10.24	0.492	20	1
32.50	10.00	0.488	30	1
31.94	10.06	0.490	40	1
32.00	10.22	0.490	50	1
32.00	10.08	0.488	60	1

## 2.2 Quasi-static shear–compression tests

In order to study the deformation and yield behavior of closed-cell aluminum foams, combined shear–compression experiments are performed on a material testing machine TAW–2000 (produced by Rising Sun Testing Instrument Co., Ltd., Changchun, China), by employing a pair of short cylindrical bars with beveled ends to apply combined shear–compression loading in the foam specimens. The cylindrical foam specimens are placed between the two parallel bevels directly, as shown in Fig. 1. A column sleeve, which is made of industrial Teflon, is used to fix the whole loading device. It is worth mentioning that the friction coefficient between the two beveled bars and the specimen is large enough, so that no slippage will

occur in the process of loading. Thus, when the bevel bars move vertically the specimen will be loaded and a combined shear–compressive loading state is achieved. Different loading conditions can be achieved by using pairs of beveled bars of different bevel angles. The loading angle  $\beta$  is introduced to denote the angle of the loading direction to the normal direction of the specimens, as illustrated in Fig. 2. Six different loading angles, namely 10°, 20°, 30°, 40°, 50° and 60°, are considered in the experiments. All experiments are performed at a loading rate of 1 mm/min. Three replicated tests are conducted for each loading case, and the results indicate a good reproducibility of the

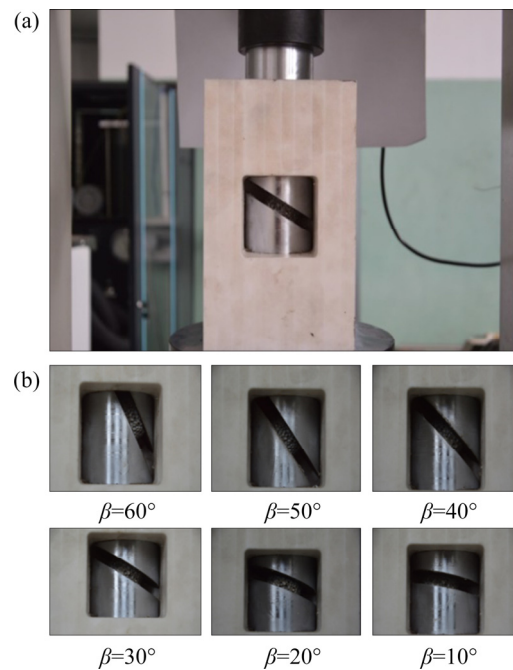


**Fig. 1** Combined shear–compression loading at different loading angles: (a) Whole view; (b) Views for different  $\beta$  values

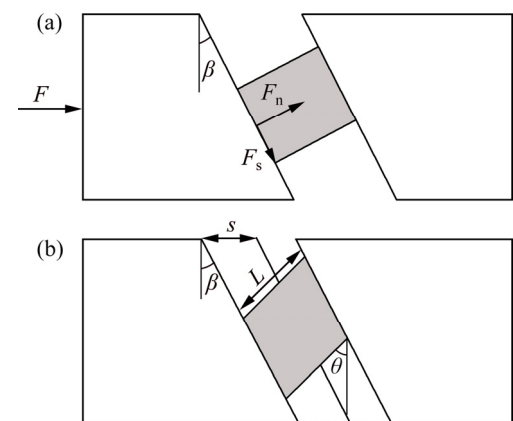


**Fig. 2** Schematic diagrams of force and deformation analyses for aluminum foam specimens: (a) Force analysis; (b) Deformation analysis

tests. Thus, the average of three experiments is taken for the comparison later.

### 2.3 Force analysis

The force analysis for foam specimens that are sandwiched between a pair of beveled bars during experiments is illustrated in Fig. 2(a).  $F$  is the total force applied on the foam specimen.  $F_n$  and  $F_s$  are the normal and tangential forces applied on the foam specimen, respectively. Thus,  $F$  can be obtained by the recorded signals in the test machine, which can be expressed as

$$F = F_n \cos \beta + F_s \sin \beta \quad (4)$$

Deformation analysis for foam specimens with no surface sliding between the two beveled bars and the foam specimen is shown in Fig. 2(b).  $L$  is the specimen height,  $\theta$  is the rotation angle of the lateral specimens surface, and  $s$  is the relative displacement of the upper and lower bevels along the loading direction. As there is no surface sliding occurs and  $s$  is small, the stress components in specimen can be estimated by [16]

$$\sigma_n = \frac{F_n}{A_n} = \frac{2(1+\nu)\cos\beta}{(1+2\nu)\cos^2\beta+1} \cdot \frac{F}{A_s} \quad (5)$$

$$\tau = \frac{F_s}{A_n} = \frac{\sin\beta}{(1+2\nu)\cos^2\beta+1} \cdot \frac{F}{A_s} \quad (6)$$

where  $\sigma_n$  is the normal stress;  $A_s$  is the cross sectional area of the foam specimens.  $\nu$  is Poisson ratio and it takes the value of 0.17 in the present study, and  $\tau$  is the shear stress. Thus, both the normal and the shear stress–strain curves can be obtained.

## 3 Experimental results

### 3.1 Load response

From the uniaxial compression, it is noted that the initial crush randomly takes place at the weakest cells firstly. Similarly, the foam cells crush randomly in the weakest region under combined shear–compression loading. However, the stress–concentrated corners in the specimens firstly collapse under combined shear–compression. Figure 3 shows the overall load–displacement responses for the closed-cell aluminum foam with the density of  $0.49 \text{ g/cm}^3$  under combined shear–compression at different loading angles. It deserves noting that a good reproducibility of the tests is

achieved and the data represented in the plot is the average of three tests for every loading case. The load–displacement response of the combined shear–compression of the aluminum foams is qualitatively similar to that in uniaxial compression and the curves consist of three regions of elastic regime, plateau regime, and densification regime. In the elastic regime, the vertical force versus displacement curve is initially linear, but becomes non-linear at the following short stages due to the loss of stiffness caused by the elastic buckling of cell walls. The initial elastic regime is followed by a peak load, which indicates the onset of the plastic collapse of the cell walls and is defined as the yield load of aluminum foams. The long plateau is extremely important for the foam application as energy absorbing devices, and is featured by the plastic plateau stress  $\sigma_{pl}$ . As shown in Fig. 3, the slope of the elastic regime before it reaches the yield point varies with loading angle. Moreover, aluminum foams exhibit increasing post-yield softening as the loading angle decreases.

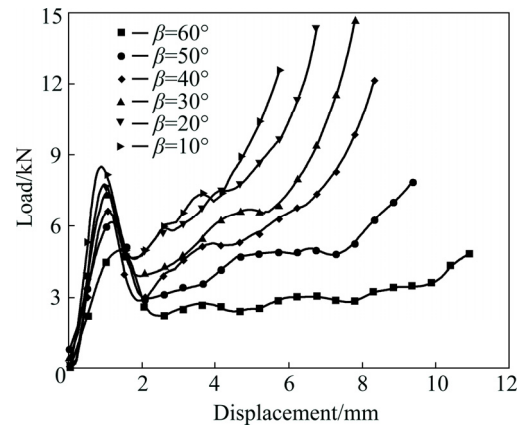


**Fig. 3** Overall load–displacement curves for aluminum foams under shear–compression loads at different loading angles

In order to determine the plateau load of aluminum foams under combined shear–compression loading, the onset displacement of densification,  $s_d$ , should be firstly obtained. According to the maximum energy absorption efficiency function criterion,  $s_d$  is defined as the displacement at which the energy absorption efficiency function reaches a maximum on the energy absorption efficiency–displacement curve, that is where the maximum of  $F^{-1} \int_0^s F(s) ds$  occurs, here,  $F$  is the load and  $s$  is the displacement.

The energy absorption efficiency–displacement curves for aluminum foams under combined shear–compression at different loading angles are shown in Fig. 4. Then, the plateau load  $F_{pl}$  of aluminum foams is then calculated by [26]

$$F_{pl} = \frac{1}{s_d - s_y} \int_{s_y}^{s_d} F(s) ds \quad (7)$$

where  $s_y$  is the yield displacement corresponding to the displacement value at yield load.

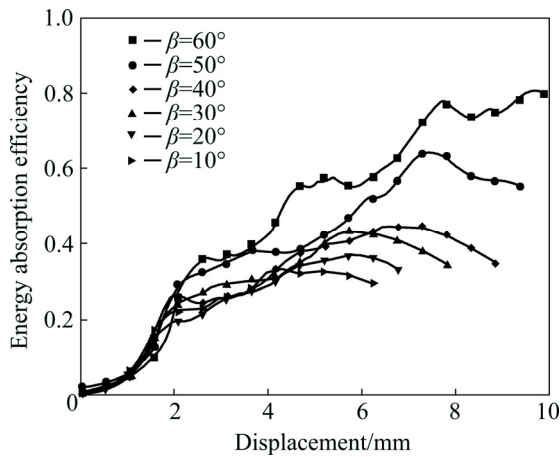


Fig. 4 Energy absorption efficiency curves of aluminum foams at different loading angles

The yield loads and plastic plateau loads of the aluminum foams at six different loading angles are shown in Fig. 5. It can be seen that, yield load decreases with the increase of loading angle, which indicates much easier yield of aluminum foams at large loading angles. Figure 5 also indicates that, the plastic plateau load decreases gradually with increasing loading angle. This is mainly due to the increase of the shear component and the shear

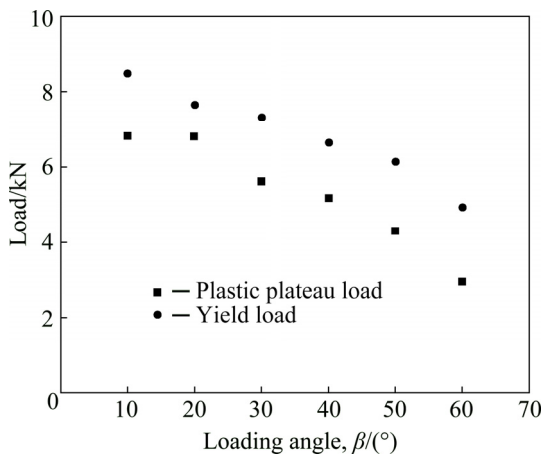


Fig. 5 Yield load and plastic plateau load at different loading angles

strength and stiffness of aluminum foams are lower than the compressive strength and stiffness.

### 3.2 Normal and shear components

The present study is focused mainly on the initial yield behaviour of aluminum foams. Using Eqs. (5) and (6), the normal stress and the shear stress are decomposed. As a result, the constitutive relationships are obtained both in the normal direction and in the tangential direction, as shown in Fig. 6. Normal yield stress decreases whereas shear yield stress increases with increasing loading angle, as can be seen from Fig. 6. It also indicates that, all normal yield stress–normal strain curves develop with almost the same slope before yield points. However, the initial slope of the shear yield stress–normal strain curves decreases as loading angle increases.

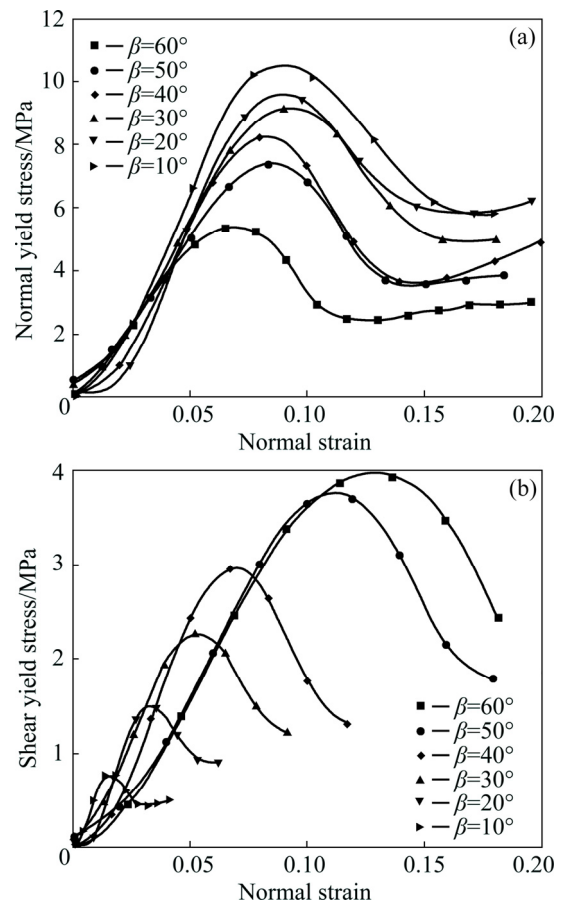


Fig. 6 Normal and shear yield stress–strain curves of aluminum foams: (a) Normal stress–strain curves; (b) Shear stress–strain curves

Under shear–compression stress state, the equivalent stress  $\sigma_e$  and mean stress  $\sigma_m$  can be estimated from

$$\begin{cases} \sigma_e = \sqrt{\sigma^2 + 3\tau^2} \\ \sigma_m = \frac{\sigma}{3} \end{cases} \quad (8)$$

The normal yield stress and shear yield stress of aluminum foams at different loading angles can be obtained from Fig. 6 and are illustrated in Fig. 7, together with the von Mises equivalent stress. As seen from Fig. 7, the strength of aluminum foams reduces with increasing loading angle, both in terms of compressive strength and equivalent strength. With the loading angle increasing from 10° to 60°, the normal yield stress decreases from 10.59 to 5.36 MPa (a 49.39% decrease) and the corresponding shear yield stress increases from 0.79 to 3.98 MPa (a 80.15% increase).

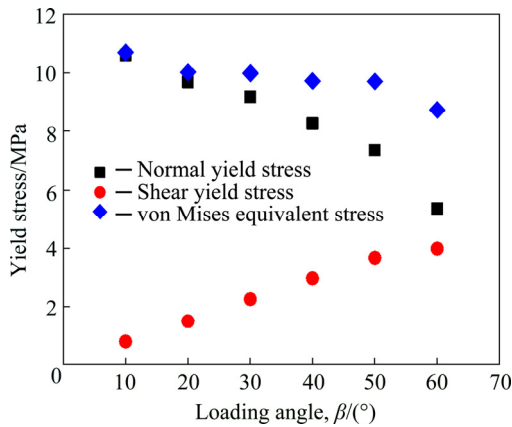


Fig. 7 Yield stress at different loading angles for combined shear–compression tests

### 3.3 Comparison of theoretical yield criterion and experimental yield surface

The yield surfaces for aluminum foams under different loading scenarios are presented in the shear–normal stress space, as plotted in Fig. 8. The theoretical yield criteria proposed by GIBSON et al (Gibson criterion) [20], MILLER (Miller

criterion) [21], DESHPANDE and FLECK (Deshpande–Fleck criterion) [22] are obtained by using the experimental results and are illustrated in Fig. 8 for comparison, of which the specific expressions are given in Table 2. The plastic Poisson ratio is assumed to be 0.17 for the aluminum foams in the present study just as mentioned before.

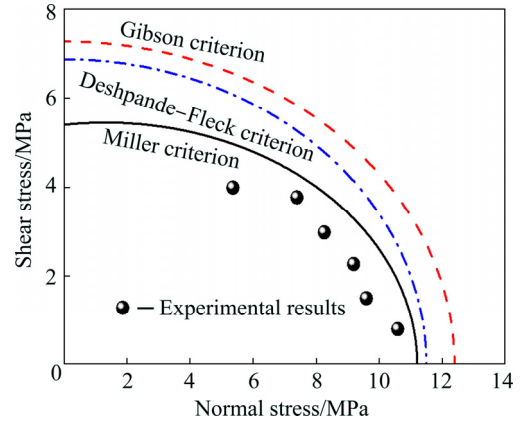


Fig. 8 Yield surfaces of aluminum foams in shear–normal stress space

Deshpande–Fleck criterion and Gibson criterion overestimate experimental yield stresses of the aluminum foams. However, Miller yield criterion is in general agreement with the experimental results. The reason is thought to be that, Miller yield criterion takes the asymmetry of uniaxial tensile strength and compressive yield strength into account, as well as the plasticity compressibility of aluminum foam materials.

## 4 Numerical simulation

### 4.1 Numerical simulation model

In order to further understand the biaxial behaviors of closed-cell aluminum foams, LS-DYNA is employed to simulate the combined

Table 2 Expressions of yield criteria and fitting results

Yield criterion	Original form	Rational fitting results
Gibson criterion	$\pm \frac{\sigma_e}{\sigma_{pl}} + 0.81 \left( \frac{\rho_f}{\rho_s} \right) \left( \frac{\sigma_m}{\sigma_{pl}} \right)^2 = 1$	$\pm \frac{\sqrt{\sigma^2 + 3\tau^2}}{12.341} + 0.000105\sigma^2 = 1$
Miller criterion	$\sigma_e - \gamma p + \frac{\alpha'}{d_0 \sigma_c} p^2 - d_0 \sigma_c = 0$	$\sqrt{\sigma^2 + 3\tau^2} - 0.128\sigma - 0.00336\sigma^2 - 9.35 = 0$
Deshpande–Fleck criterion	$\frac{1}{1 + (\alpha/3)^2} [\sigma_e^2 + \alpha^2 \sigma_m^2] - \sigma_y^2 = 0$	$\frac{\tau^2}{47.223} + \frac{\sigma^2}{132.125} = 1$

$\sigma_{pl}$  is the uniaxial yield strength,  $\sigma_{pl} = (\sigma_c + \sigma_t)/2$ ,  $\sigma_t$  is tensile strength, respectively. The parameters  $\gamma$ ,  $\alpha'$  and  $d_0$  are determined by  $\beta_1 = \sigma_c/\sigma_t$  and plastic Poisson ratio  $\gamma_{pl}$ . The  $\alpha$  of the yield surface is determined by the plastic Poisson ratio of the aluminum foam

shear–compression behaviors based on the tetrakaidecahedron model. The cell size of the tetrakaidecahedron is 2 mm and the cell wall thickness is 0.084 mm. Thus, the corresponding density of the closed-cell aluminum foam is  $0.49 \text{ g/cm}^3$ , which is just the same as that of the foam materials used in the experiments. The numerical models are shown in Table 3.

**Table 3** Material and material models for elements

Part name	Material	Density/ ( $\text{g}\cdot\text{cm}^{-3}$ )	Material model
Upper beveled bar	45# steel	7.83	RIGID
Lower beveled bar	45# steel	7.83	RIGID
Cell wall material	Aluminum alloy	2.70	PLASTIC_KINEMA TIC with elastic modulus $E=69 \text{ GPa}$ , and tangent modulus $G=26.5 \text{ GPa}$

In the present study, a constant loading rate virtual test under combined shear–compression is performed. The closed-cell foam specimen is placed between two beveled bars, as depicted in Fig. 9. Simulation results show that macroscopic properties of the closed-cell aluminum foam can be well simulated by using a stacking model of  $3 \times 3 \times 3$  repeated fixed pore structures. Therefore, the numerical model established in the present study is a stacking model of  $7 \times 7 \times 5$  pore structures. The lower beveled bar is fixed and the upper beveled bar is set as a loading end with a constant velocity at a loading angle  $\beta$ . The friction between the sleeve and the beveled bars is ignored in the model. By defining the rough friction constrain a general contact with a friction coefficient of 0.02 is defined for the whole model to make sure the fact that no slip occurs, except the interface between the loading bar and the foam specimen. As long as the ratio of kinetic energy to internal energy and the ratio of hourglass energy to internal energy in the simulation are less than 5%, the entire loading process can be treated as a quasi-static process. Thus, the computation time can be shortened by increasing the loading rate in the simulation. Therefore, a loading rate of 0.03 m/s is applied on

the upper beveled bar in the simulation. The simulation results of combined shear–compression at different loading angles are also shown in Fig. 9.

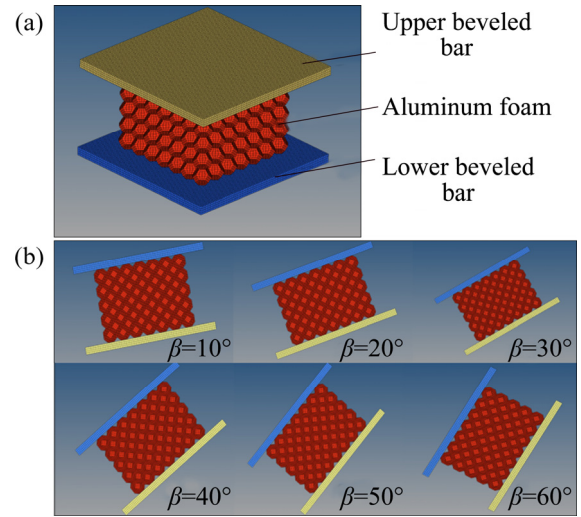


**Fig. 9** Finite element model under combined shear–compression loading (a) and scenarios at different loading angles (b)

#### 4.2 Verification of numerical results

Due to that the plastic deformation of aluminum foams is highly localized, pressure–displacement curves are used to characterize the overall material responses. The pressure  $p$  is estimated by dividing the load  $F$  in the vertical direction with the specimen cross-section area  $A_s$ . The overall pressure–displacement curves are determined from the numerical results and compared with those from the experiments. The experimental and numerical pressure–displacement curves under combined shear–compression at a loading angle of  $\beta=50^\circ$  are depicted in Fig. 10, together with those under uniaxial compression. The numerical overall pressure–displacement curves agree reasonably well with the experimental results.

Comparisons of initial yield stress and plateau stress at different loading angles are presented in Fig. 11. Here, the plateau stress is defined as

$$\sigma_{pl} = \frac{1}{s_d - s_y} \int_{s_y}^{s_d} p ds \quad (9)$$

A maximum difference of only 8.2% between the numerical and experimental initial yield stress is found at the loading angle of  $30^\circ$ . The plateau stresses obtained from numerical simulation are in good agreement with the experimental results.

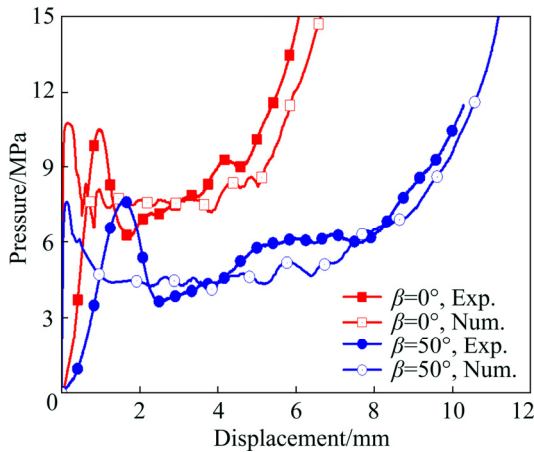


**Fig. 10** Comparison of overall pressure–displacement curves

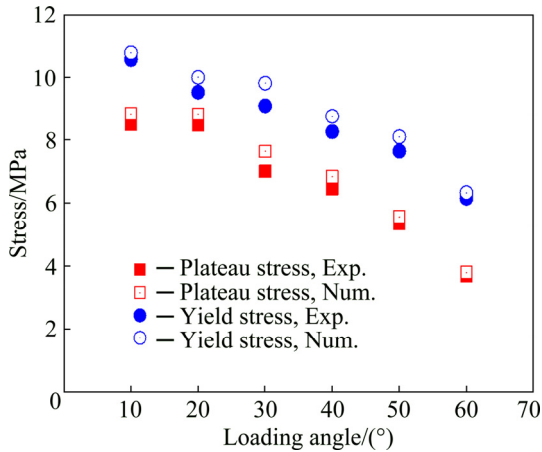


**Fig. 11** Numerical and experimental yield stress and plateau stress at different loading angles

**4.3 Analysis and comparison**

The von Mises stress distribution of the cellular specimen under combined shear–compression is shown in Fig. 12, as well as that under uniaxial compression. It can be seen that the yield process of specimen under combined shear–compression is different from that of the specimen under uniaxial compression. Yield initiates from the stress-concentrated corners in the specimens under combined shear–compression. The area circled in red in Fig. 12(b) indicates the zone where the initiation of yield occurs. For the specimen under combined shear–compression, the stress distribution at the specimen/bar interfaces is no longer uniform. As the loading angle gets larger, yield initiates earlier due to the stress concentration and the increase of shear stress component at the corners. For example, the cellular specimen under uniaxial compression yields at 7268  $\mu$ s in the

simulation, while the specimen under combined shear–compression at the loading angle of 60° yields at 6977  $\mu$ s in the simulation, which is much earlier.

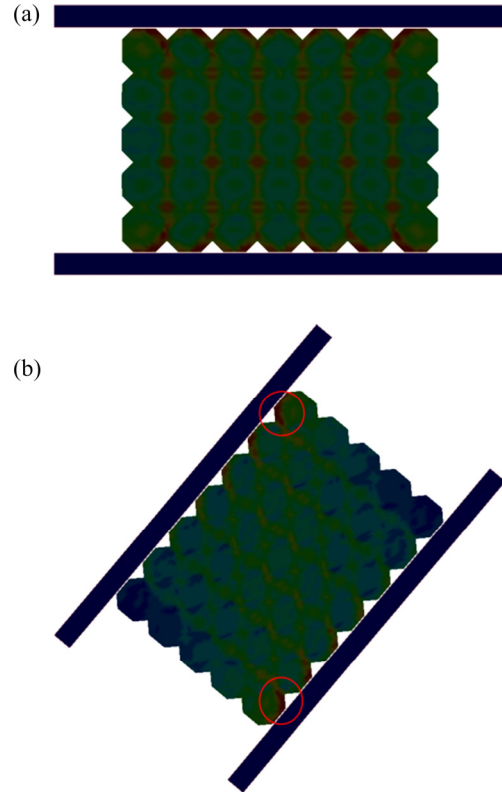


**Fig. 12** von Mises stress distribution of specimen: (a) Uniaxial compression; (b) Combined shear–compression

The yield surface is also obtained from the numerical results for comparison purpose, as shown in Fig. 13 and Fig. 14. The numerical yield surface agrees well with the experimental yield surface for the aluminum foam with the same cell size and density.

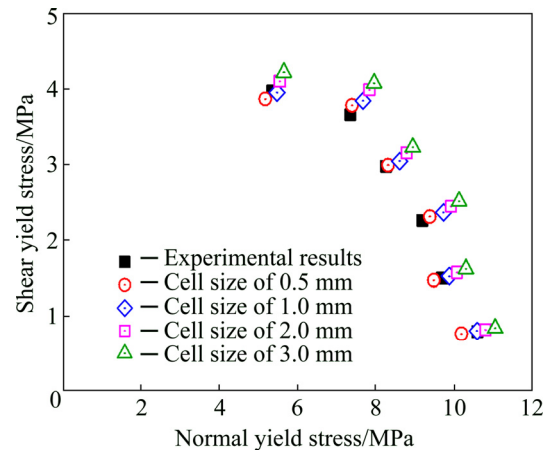


**Fig. 13** Effect of cell size on yield surface

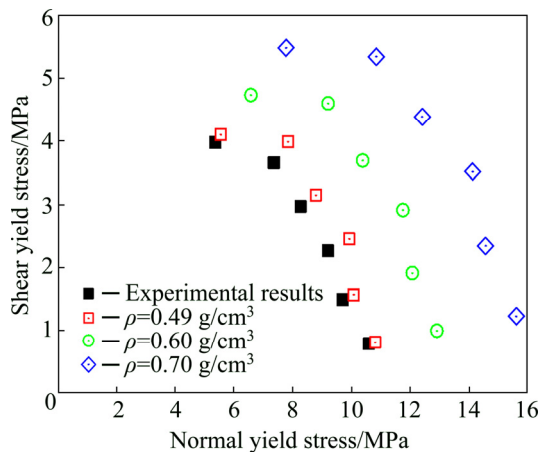


Fig. 14 Effect of foam density on yield surface

The effects of two important parameters, i.e. the cell size and the aluminum foam density, on the yield surface are also studied. In the finite element model, the aluminum foam density varies by varying the cell wall thickness of the tetrakaidcahedron. Aluminum foams of the same density with four different cell sizes of 0.5, 1.0, 2.0, and 3.0 mm are considered in the present study, of which the corresponding cell wall thickness values are 0.021, 0.042, 0.084 and 0.126 mm, respectively. The numerical results are shown in Fig. 13, together with the experimental results. In the range of cell sizes studied, the shear yield stress and normal yield stress increase with the increase of cell size. Generally, closed-cell aluminum foams are mainly composed of cell pores and cell walls. As the foam density remains constant, the larger the average cell size is, the larger the cell wall thickness is. Moreover, the yield stress is substantially proportional to the cell wall thickness. Therefore, the larger the cell size is, the higher the yield stress is.

Aluminum foams of the same cell size are adopted to study the effect of density on the yield surface with three different densities, namely 0.49, 0.60 and 0.70 g/cm<sup>3</sup>, of which the corresponding cell wall thickness values are 0.084, 0.100 and 0.120 mm, respectively. The results are shown in Fig. 14. An elliptical shape is found for the aluminum foams with each density case and the expansion of the yield locus from low to high density is almost isotropic. Figures 13 and 14 also indicate that, density of the aluminum foams is the dominant factor on their mechanical properties compared with the cell size. As the closed-cell

aluminum foams are usually used in engineering practice for cushioning and energy absorption, so the foam density may be much significant.

## 5 Conclusions

(1) The yield load and plastic plateau load of the aluminum foam reduce gradually as the loading angle increases. The introduction of shear stress component during combined shear–compression loading reduces the equivalent yield strength of the aluminum foam. The larger the loading angle is, the lower the equivalent yield strength is.

(2) Yield initiates at the stress-concentrated corners in the specimens under combined shear–compression and the stress distribution at the specimen/bar interfaces is no longer uniform. In the range of cell sizes studied, the larger the foam cell size is, the higher the yield stress is.

(3) Aluminum foam density is found to be the dominant factor on its mechanical properties compared with the cell size and is more significant in engineering practice.

## References

- [1] GIBSON L J, ASHBY M F. Cellular solids: Structure and properties [M]. Cambridge: Cambridge University Press, 1997.
- [2] WANG Ning-zhen, CHEN Xiang, LI Ao, LI Yan-xiang, ZHANG Hua-wei, LIU Yuan. Three-point bending performance of a new aluminum foam composite structure [J]. Transactions of Nonferrous Metals Society of China, 2016, 26: 359–368.
- [3] FAN Su-feng, ZHANG Tao, YU Kun, FANG Hong-jie, XIONG Han-qing, DAI Yi-long, MA Jia-ji, JIANG Da-yue, ZHU Hua-long. Compressive properties and energy absorption characteristics of open-cell nickel foams [J]. Transactions of Nonferrous Metals Society of China, 2017, 27: 117–124.
- [4] YUAN Jian-yu, LI Yan-xiang. Effects of cell wall property on compressive performance of aluminum foams [J]. Transactions of Nonferrous Metals Society of China, 2015, 25: 1619–1625.
- [5] COMBAZ E, BACCIARINI C, CHARVET R, DUFOUR W, MORTENSEN A. Multiaxial yield behaviour of Al replicated foam [J]. Journal of the Mechanics and Physics of Solids, 2011, 59: 1777–1793.
- [6] LUO Geng, XUE Pu, SUN Shi-guang. Investigations on the yield behavior of metal foam under multiaxial loadings by an imaged-based mesoscopic model [J]. International Journal of Mechanical Sciences, 2018, 142–143: 153–162.
- [7] LI Zhi-bin, ZHENG Zhi-jun, YU Ji-lin, TANG Li-qun. Effect of temperature on the indentation behavior of closed-cell

- aluminum foam [J]. *Materials Science and Engineering A*, 2012, 550: 222–226.
- [8] LI Zhi-bin, ZHENG Zhi-jun, YU Ji-lin, YANG Jie, LU Fang-yun. Spherical indentation of closed-cell aluminum foams: An empirical force–depth relation [J]. *Materials Science and Engineering A*, 2014, 618: 433–437.
- [9] RUAN D, LU G, ONG L S, WANG B. Triaxial compression of aluminium foams [J]. *Composites Science and Technology*, 2007, 67: 1218–1234.
- [10] ZHOU Zhi-wei, WANG Zhi-hua, ZHAO Long-mao, SHU Xue-feng. Loading rate effect on yield surface of aluminum alloy foams [J]. *Materials Science and Engineering A*, 2012, 543: 193–199.
- [11] ZHOU Zhi-wei, WANG Zhi-hua, ZHAO Long-mao, SHU Xue-feng. Uniaxial and biaxial failure behaviors of aluminum alloy foams [J]. *Composites Part B: Engineering*, 2014, 61: 340–349.
- [12] KOSSA A. A new biaxial compression fixture for polymeric foams [J]. *Polymer Testing*, 2015, 45: 47–51.
- [13] MOSLEH Y, BOSCHE K V, DEPREITERE B, SLOTEN J V, VERPOEST I, IVENS J. Effect of polymer foam anisotropy on energy absorption during combined shear compression loading [J]. *Journal of Cellular Plastics*, 2018, 54: 597–613.
- [14] ZHAO Peng-duo, LU Fang-yun, LIN Yu-liang, CHEN Rong, LI Jun-lin, LU Li. Technique for combined dynamic compression–shear testing of PBXs [J]. *Experimental Mechanics*, 2012, 52: 205–213.
- [15] ZHOU Zhi-wei, SU Bu-yun, WANG Zhi-hua, LI Zhi-qiang, SHU Xue-feng, ZHAO Long-mao. Shear-compression failure behavior of PMMA at different loading rates [J]. *Materials Letters*, 2013, 109: 151–153.
- [16] XU Song-lin, HUANG Jun-yu, WANG Peng-fei, ZHANG Chao, ZHOU Li-jiang, HU Shi-sheng. Investigation of rock material under combined compression and shear dynamic loading: An experimental technique [J]. *International Journal of Impact Engineering*, 2015, 86: 206–222.
- [17] BOOMSMA K, POULIKAKOS D. On the effective thermal conductivity of a three-dimensionally structured fluid-saturated metal foam [J]. *International Journal of Heat and Mass Transfer*, 2001, 44: 827–836.
- [18] MILLS N J, ZHU H X. The high strain compression of closed-cell polymer foams [J]. *Journal of the Mechanics and Physics of Solids*, 1999, 47: 669–695.
- [19] GRENESTEDT J L. Effective elastic behavior of some models for ‘perfect’ cellular solids [J]. *International Journal of Solids and Structures*, 1999, 36: 1471–1501.
- [20] GIBSON L J, AHSBY M F, ZHANG J, TRIANTAFILLOU T C. Failure surfaces of cellular materials under multiaxial loads. I: Modelling [J]. *International Journal of Mechanical Sciences*, 1989, 31: 635–663.
- [21] MILLER R E. A continuum plasticity model for the constitutive and indentation behaviour of foamed metals [J]. *International Journal of Mechanical Sciences*, 2000, 42: 729–754.
- [22] DESHPANDE V S, FLECK N A. Isotropic constitutive models for metallic foams [J]. *Journal of the Mechanics and Physics of Solids*, 2000, 48: 1253–1283.
- [23] LI Zhi-bin, ZHENG Zhi-jun, YU Ji-lin. Low-velocity perforation behavior of composite sandwich panels with aluminum foam core [J]. *Journal of Sandwich Structures and Materials*, 2012, 15: 92–109.
- [24] TEKOGULU C, GIBSON L J, PARDOEN T, ONCK P R. Size effects in foams: Experiments and modeling [J]. *Progress in Materials Science*, 2011, 56: 109–138.
- [25] ANDREWS E W, GIOUX G, ONCK P R, GIBSON L J. Size effects in ductile cellular solids. Part II: Experimental results [J]. *International Journal of Mechanical Sciences*, 2001, 43: 701–713.
- [26] LI Zhi-bin, ZHENG Zhi-jun, YU Ji-lin, YANG Jie. Indentation of composite sandwich panels with aluminum foam core: An experimental parametric study [J]. *Journal of Reinforced Plastics and Composites*, 2014, 33: 1671–1681.

## 闭孔泡沫铝在压剪加载下的双向力学行为

李志斌<sup>1</sup>, 李雪艳<sup>1</sup>, 郑宇轩<sup>2</sup>

1. 国防科技大学 文理学院, 长沙 410073;

2. 北京理工大学 爆炸科学与技术国家重点实验室, 北京 100081

**摘要:** 为了研究闭孔泡沫铝合金在双轴加载下的屈服行为, 对一种闭孔泡沫铝在较宽的加载角度范围开展压剪复合加载试验和数值模拟研究。压剪复合加载通过加入一对斜端面垫块和一个长方体套筒来实现。测试屈服面, 并与多个理论模型推导得到的屈服面进行比较。通过将闭孔泡沫铝的多孔结构建模成十四面体, 对其双轴加载行为进行有限元模拟。结果表明, 在压剪复合加载试验条件下, 闭孔泡沫铝的屈服从试件应力集中的角上开始, 而且试样/垫块接触面的应力分布不再均匀。在所研究的加载角度范围内, 胞元尺寸越大, 屈服应力越大。泡沫铝合金的密度相对于孔径尺寸来说是影响其力学行为的主导因素, 因而在工程应用中也显得更加重要。

**关键词:** 压剪复合加载; 闭孔泡沫铝; 屈服面; 双轴加载; 屈服行为

(Edited by Wei-ping CHEN)